Complementary p- and n-Type Polymer Doping for Ambient Stable Graphene Inverter

Je Moon Yun,[†,‡,∥] Seokhan Park,[‡,∥] Young Hwan Hwang,[‡] Eui-Sup Lee,[†,§] Uday Maiti,[†,‡] Hanul Moon,[⊥] Bo-Hyun Kim,[‡] Byeong-Soo Bae,[‡] Yong-Hyun Kim,[†,§,*] and Sang Ouk Kim[†,‡,*]

[†]Center for Nanomaterials and Chemical Reactions, Institute for Basic Science (IBS), Daejeon 305-701, Republic of Korea, [‡]Department of Materials Science and Engineering, KAIST, Daejeon 305-701, Republic of Korea, [§]Graduate School of Nanoscience and Technology, KAIST, Daejeon 305-701, Republic of Korea, and [⊥]Department of Electrical Engineering, KAIST, Daejeon 305-701, Republic of Korea. [∥]J. M. Yun and S. Park contributed equally.

ABSTRACT Graphene offers great promise to complement the inherent limitations of silicon electronics. To date, considerable research efforts have been devoted to complementary p- and n-type doping of graphene as a fundamental requirement for graphene-based electronics. Unfortunately, previous efforts suffer from undesired defect formation, poor controllability of doping level, and subtle environmental sensitivity. Here we present that graphene can be complementary p- and n-doped by simple polymer coating with different dipolar characteristics. Significantly, spontaneous vertical ordering of dipolar pyridine side groups of poly(4-vinylpyridine) at graphene surface can stabilize n-type doping at room-temperature ambient condition. The dipole field also enhances and balances the charge mobility by screening the impurity charge effect from the bottom substrate. We successfully demonstrate ambient stable inverters by integrating p- and n-type graphene transistors, which demonstrated clear voltage inversion with a gain of 0.17 at a 3.3 V input voltage. This straightforward polymer doping offers diverse opportunities for graphene-based electronics, including logic circuits, particularly in mechanically flexible form.

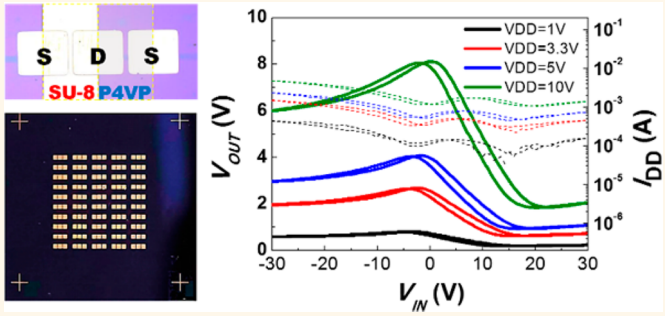

KEYWORDS: graphene · FET · inverter · doping · polymer

As the advance of silicon electronics relying on simple dimensional downscaling faces inherent limitations, graphene is emerging as an alternative or complementary electronic material.[1,2] Along with the mechanically flexible and optically transparent atomic-scale dimension, the extraordinary electronic properties of graphene, including massless Dirac fermion behavior of charge carriers,[3] ambipolar electric field effect,[4] and quantum Hall effect,[5] offer new opportunities for next-generation electronics. In recent years, there has been noticeable progress toward the realization of integrated circuits based on graphene, including integrated ring oscillators[6] and nonvolatile switching devices.[7] For the ultimate realization of graphene-based electronics, a robust and controllable complementary p- and n-type doping method is a crucial prerequisite.

Foreign element doping may provide excess charge carriers in semiconductors. This simple principle is the key technology to manipulate the local carrier density and conductivity of electronic devices. The fundamental functions of electronic devices, such as rectification and transistor switching, generally require a robust and area-selective doping process with tunable doping level.[8] To date, a few doping methods have been exploited for graphene, including substitutional doping,[9−11] electrostatic doping by external field,[12] and charge transfer doping.[13−17] Unfortunately, these approaches reveal intrinsic drawbacks, such as undesired defect formation, complex processing steps, and subtle sensitivity to environment. More significantly, ambient stable complementary p- and n-type doping with compatibility with conventional device fabrication has hardly been demonstrated yet.

In this work, we report ambient stable complementary p- and n-type polymer

* Address correspondence to sangouk.kim@kaist.ac.kr, yong.hyun.kim@kaist.ac.kr.

Received for review October 11, 2013 and accepted December 18, 2013.

Published online December 18, 2013
10.1021/nn4053099

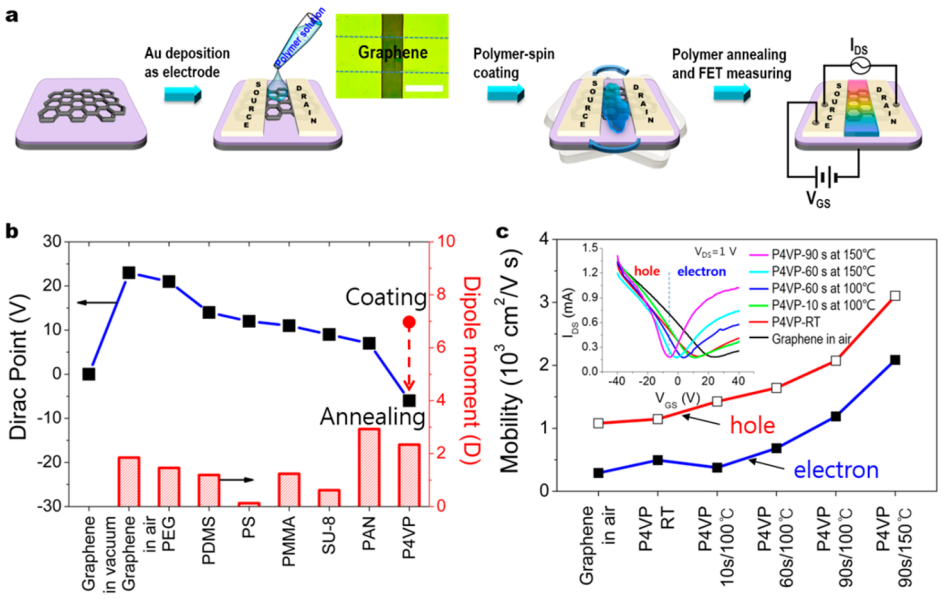

Figure 1. Dirac point (DP) tuning of polymer-doped graphene FETs (GFETs). (a) Schematic illustration of polymer-doped GFET fabrication. The optical microscopy image shows a GFET fabricated on a 300 nm SiO_2 silicon wafer. Scale bar is 100 μm. (b) DP variation with different dipolar polymer coatings. The right axis indicates dipole moments of coated polymers presented by red bars. The red arrow indicates the negative shift of DP for P4VP-doped graphene with thermal annealing. (c) Variation of hole- and electron-mobility of P4VP-doped graphene with thermal annealing. All FET performances were measured at room-temperature ambient conditions.

doping of graphene and its application to a graphene inverter.[18−20] Highly stable graphene doping is achieved by simple coating of dipolar polymer films onto a pristine graphene surface. While conventional polymers with different dipolar characteristics enable the precise tunability of doping level, poly(4-vinylpyridine) (P4VP) imposes a strong dipole field[21] to yield an n-type doping, highly stable at ambient conditions. Moreover, the dipole field can dramatically improve and balance the carrier mobility by screening the impurity charge effect from the bottom SiO_2 substrate.[22] Taking advantage of complementary p- and n-doping with different polymers, ambient stable inverters are fabricated by area-selective doping in conjunction with conventional photolithography. The inverter devices employing a back gate regime demonstrated robust inverting performance with clear voltage inversion and a voltage gain of 0.17 at a 3.3 V input voltage under ambient air condition.

RESULTS AND DISCUSSION

An atomically thin graphene monolayer (Supporting Figure S1) is generally sensitive to the perturbations from surface charges and adsorbed molecules.[22,23] We systematically investigated the surface doping effects from various polymers with different polar characteristics (see Supporting Table S1 for the dipole moments of the polymers calculated by *ab initio* theory). As schematically illustrated in Figure 1a, field effect transistor (FET) structures were fabricated to characterize the modulation of electronic properties by polymer doping (see Experimental Methods section for details). Polymer doping layers were spin-casted onto the graphene channel between Au electrodes and thermally annealed at 100−150 °C. The device characteristics are measured at room temperature in air. Owing to the unusual band structure, the graphene FET (GFET) exhibits ambipolar conduction.[24,25] Unlike unipolar silicon complementary metal-oxide-semiconductor (CMOS) devices, where doping species determine p- or n-type behavior, a GFET is switchable from p-type to n-type with gate bias modulation.[26,27]

Figure 1b (and Supporting Figures S2 and S3) shows the variation of the Dirac point (DP) influenced by the dipolar characteristics of polymer doping layers. In a vacuum, hydrocarbon polymers, such as polystyrene (PS), is known to have no noticeable doping effect, while other polymers with strong dipoles usually show a weak p-type doping effect. In our air ambient condition measurements, most of the polymer dopants lead to p-doped characteristics regardless of dipolar strength. However, the p-doping effect is weaker than that of pristine GFET exposed to air (DP of 23 V),[28] due to the less polar characteristics of polymers than moisture or oxygen molecules absorbed on the graphene surface under air ambient condition. Interestingly, while the DPs of other polymer-doped graphene remained in the positive V_{GS} range, the DP of P4VP-coated graphene shifted down to a negative V_{GS} of −6 V after thermal annealing. (See Supporting Figure S4; a thicker P4VP-coated GFET is more downshifted to −17 V.) Thermal annealing also increased the mobility of both electron and hole carriers, as plotted in Figure 1c. The electron mobility from the n-branch

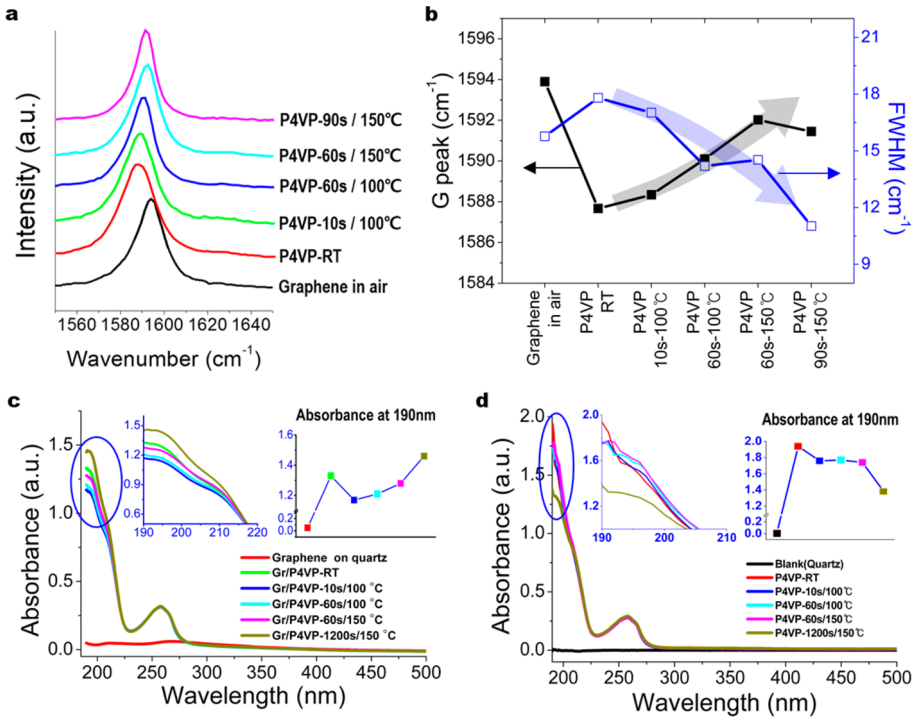

Figure 2. Raman and UV−vis spectra of P4VP-doped graphene. (a) G peak Raman spectra for bare graphene and P4VP-coated graphene with different annealing conditions. (b) Variations of G peak position (solid squares) and fwhm's (open squares) with annealing condition. Raman spectroscopy was measured using a 514 nm laser source. UV−vis absorbance spectra of P4VP films (c) deposited on graphene and (d) without graphene.

increased from 291 to 2087 $cm^2\ V^{-1}\cdot s^{-1}$, while the hole mobility from the p-branch increased from 1081 to 3105 $cm^2 V^{-1}\cdot s^{-1}$ (Supporting Figure S5 and Table S2).[29] More significantly, this polymer doping effect is highly stable at ambient condition. The measured device characteristics are highly stable at ambient condition for more than two weeks (Supporting Figure S6).

Raman spectroscopy is widely utilized for structural characterization of graphene.[30,31] As shown in Figure 2a and b, the G peak of air-exposed graphene, which corresponds to the E_{2g} phonon at the Brillouin zone center, is located at 1594 cm^{-1} with the strong doping effect from the oxygen and moisture in the air.[32] (The G peak is calculated to be at 1580 cm^{-1} for bare graphene without gas absorption.[31]) When the P4VP layer was deposited onto the graphene surface, the G peak was downshifted to 1587 cm^{-1}. This variation is attributed to dissipation of the doping effect from oxygen or water molecules by the less polar polymer coating. When the annealing time and temperature increases, the G peak is gradually upshifted. The width of the G peak, which is another indication of doping[33] or strain[34] to graphene, also becomes narrow with thermal annealing.[35]

We also performed UV−vis spectroscopy measurements to characterize the excitation of π-electrons and nonbonding (n) electrons of P4VP.[36] While pure graphene was almost transparent down to 190 nm wavelength, the P4VP-doped graphene showed two absorbance peaks. The peaks at 190 and 258 nm correspond to the excitation of π-electrons in the C=C double bond and n-electrons of the N atom in the pyridine ring to higher π^* antibonding molecular orbitals, respectively. The peak at 190 nm gradually grows with annealing time (inset of Figure 2c). In the control experiment for the P4VP film without graphene (inset of Figure 2d), however, there is no noticeable change with thermal annealing. In general, the absorbance at a particular wavelength increases with the number of molecules or groups associated with the transitions. The UV−vis spectroscopy results suggest that the transition of π-electrons in P4VP to the π^* antibonding level is strongly influenced by the presence of graphene. Both Raman and UV−vis spectroscopy demonstrate that the pyridinic ring and graphene show a close interaction, which becomes stronger with thermal annealing.

Microscopic origin of the n-doping effect from P4VP was investigated by the first-principles electronic structure calculations of pyridine- and P4VP-coated graphene systems based on the density-functional theory (DFT) formulation.[37−39] Pyridine is a polar molecule containing an N atom in the benzene-like hexagon and is alternatively attached on every two backbone C atoms of the P4VP polymer, as shown in Figure 3a (syndiotactic chain configuration was assumed to represent a local chain arrangement of P4VP). Because of steric hindrance between the neighbor pyridine rings in P4VP, the pyridine group is likely to be perpendicularly aligned to the backbone direction. When one pyridine ring is rotated by 90°, the DFT total energy is increased

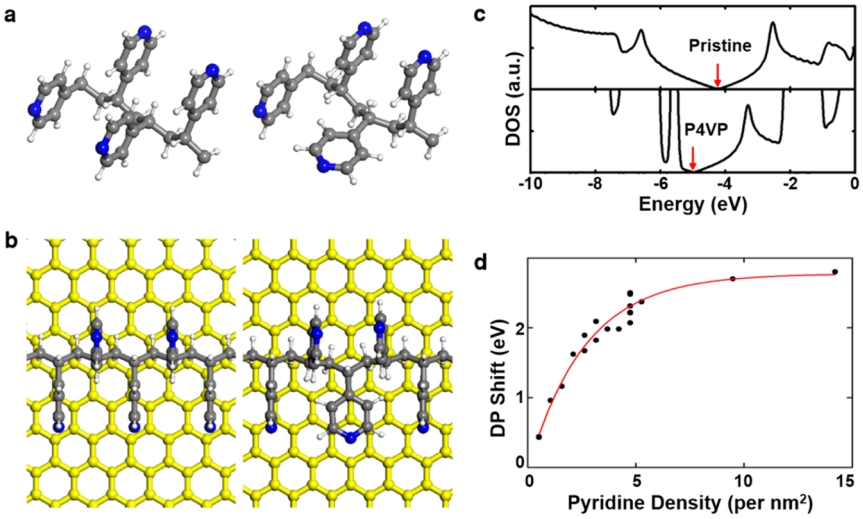

Figure 3. Atomistic model for dipolar P4VP doping. Energy minimum segmental conformations of (a) free P4VP polymer segment and (b) its ordering at the graphene surface. Gray, blue, and white colored balls represent C, N, and H atoms, respectively. Graphene is colored in yellow for contrast. (c) Density of states (DOS) of pristine graphene and P4VP-doped graphene. Red arrows indicate the DP position, and the energy zero is the vacuum level. (d) DP shift as a function of pyridine areal density on graphene. Red curve is a guide for the eye.

by 0.37 eV. Subsequently, when P4VP is adsorbed on the graphene surface as in Figure 3b, the adsorption energy is calculated to be 0.65 and 0.83 eV, respectively, for the ideal and rotated P4VP models. The enhanced adsorption energy of the rotated P4VP model can be understood in terms of the $\pi-\pi$ interaction, which is larger than the CH$-\pi$ interaction, between the pyridine ring and graphene plane (Supporting Figure S7). Atactic P4VP polymers are amorphous at ambient conditions. However, due to the CH$-\pi$ and $\pi-\pi$ interactions between the pyridine groups and graphene plane, the P4VP segments may undergo local ordering on graphene during the annealing process, as shown in Figure 3b. Significantly, direct first-principles DFT calculation demonstrates that when the P4VP segment is ordered on the graphene surface, half of the pyridine rings in P4VP are vertically aligned, and this creates a strong dipole field.[40,41] This dipole field downshifts the DP of P4VP-coated graphene by 0.77 eV, as shown in Figure 3c, which is consistent with our experimental observation. It is noteworthy that when the pyridinic ring is aligned parallel to graphene, there is no significant DP shift. Since the local electrostatic potential of pyridine molecules does not change along the perpendicular direction of the graphene surface, the DP remains at the same position with pristine graphene.

Because DP shift is attributed to the dipole field from vertically aligned pyridines, the degree of DP shift should depend on the areal density of vertically aligned pyridines. The DP shift was checked with the gradual increase of pyridine coverage on graphene, as shown in Figure 3d (Supporting Figure S8). When the graphene surface is fully covered with vertically aligned pyridines up to one monolayer (5 molecules per nm^2), the negative DP shift was 2.3 eV. If pyridine molecules are further stacked on graphene as a multilayer, the DP no longer shifts but saturates at 2.8 eV. Taken together, the DP shift with thermal annealing can be attributed to the increased areal density of graphene-induced ordering of P4VP segments. Interestingly, this dipole field effect also enhances and balances the carrier mobility within the graphene plane, as shown in Figure 1c. Carrier mobility of the graphene on the SiO_2 substrate is known to be deteriorated by the extrinsic scattering from charge impurity or the phonon mode of the SiO_2 surface.[42−44] In particular, unavoidable impurity charges at the SiO_2 surface with a concentration as high as $\sim 10^{11}$/cm^2 may create a charge puddle in the graphene plane. Recently, it has been reported that the dipole field from a dielectric medium on graphene may screen the Coulombic potential from the impurity charges.[45,46] This dipolar effect can also balance the mobility for electron and hole carriers. Unbalanced scattering for electrons and holes by the impurity charges can be relieved by this screening effect.[44] As plotted in Figure 1c, while the hole mobility was 3.71 times higher than electron mobility before dipolar ordering, this asymmetry gradually decreases with thermal annealing down to 1.49.

As a representative example of device application, our polymer doping can be exploited for a graphene inverter device. As demonstrated above, an air-exposed undoped graphene transistor generally shows p-type behavior under ambient conditions. To date, n-type graphene transistors have been realized by the charge transfer doping from electron-donating materials, such as titanium suboxide,[17] potassium,[47] polyethyleneimine (PEI),[15] hydrazine,[10] and viologen.[48] However, oxidative, hygroscopic, or liquid phase dopants frequently reveal an unstable doping effect

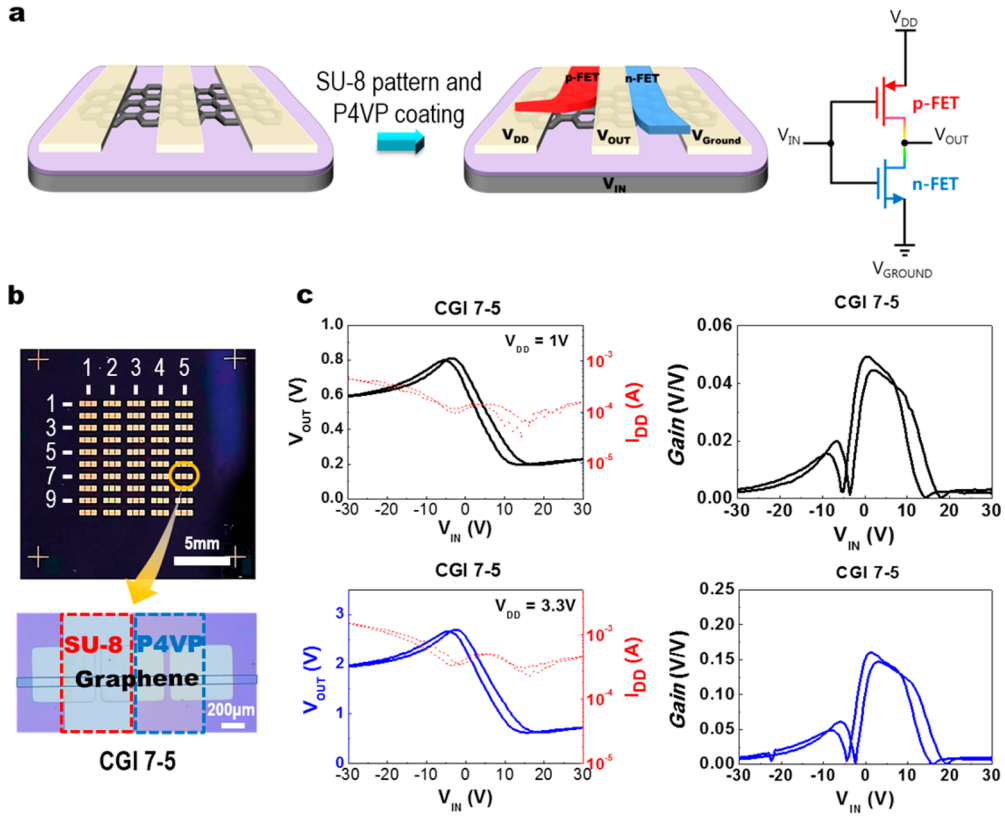

Figure 4. Complementary graphene inverter (CGI) performances. (a) Schematic illustration of complementary graphene inverter and circuit layout. (b) Optical microscopic images of 50 graphene inverters (top) and a magnified unit (bottom). Red-dashed box indicates SU-8-doped p-type GFET area, whereas blue-dashed box indicates P4VP-doped n-type GFET area, respectively. (c) Typical electrical switching characteristics (at V_{DD} = 1 and 3.3 V) of CGIs.

under ambient conditions. For instance, liquid PEI readily absorbs moisture, CO_2, or O_2 gas at air ambient conditions, which gradually degrades the n-doping effect.[15,49] Due to the technological hardship for ambient stable n-doping, graphene inverter fabrication has relied on p-type-only devices thus far. By contrast, our n-doping from solid P4VP ensures highly stable n-doping based on the spontaneously ordered dipolar segments at the graphene surface. Our approach possesses many advantages over previous methods, including mechanical robustness arising from the high glass transition temperature (~140 °C) of P4VP, cost effectiveness, and facile solution-based processing. Notably, there is no chemical reaction nor electrical degradation of graphene during our polymer-based doping. Besides, a conventional device fabrication process involved with O_2-RIE and photolithography is highly compatible with our approach, which is advantageous for complex integrated device fabrication.

Integration of p- and n-type graphene transistors complements field-effect inverters. After patterning a graphene sheet into 100 μm width by masked O_2-RIE etching, the source and drain electrodes were deposited by masked thermal evaporation of Au (Figure 4a and Supporting Figure S9). For p-type doping, a negative tone photoresist (SU-8) was patterned by conventional lithography. For n-type doping, P4VP was casted onto the graphene-exposed area to constitute a pull-down transistor. We note that 50 inverter devices (Figure 4b) were fabricated, and their performances are statistically analyzed (Supporting Figures S10−S13). Device performance was highly reproducible owing to the stable polymer doping at air ambient conditions.

Figure 4b shows a microscopic image of a complementary graphene inverter (CGI) array. p-Type doping from SU-8 (DP = 12 V with supply voltage V_{DD} = −1 V) and n-type doping from P4VP (DP = −6 V with V_{DD} = −1 V) are integrated for their complementary behaviors (Supporting Figure S11). Figure 4c shows the typical electrical switching characteristics at air ambient condition (for CGI 7−5, the I_{DS} values of p- and n-type FETs at V_D = 1 and 3.3 V are similar, as shown in Supporting Figure S14). The output voltage (V_{OUT}) transfer curve exhibits the maximum value at the input voltage (V_{IN}) of −6 V and the minimum value at a V_{IN} of 12 V, respectively. The increase in V_{IN} causes current delivery by n-doped FET to increase and by p-doped FET to decrease, which decreases the V_{OUT}. Consequently, the V_{IN} for the maximum V_{OUT} indicates the DP of a P4VP-coated n-type FET, whereas that for the minimum V_{OUT} indicates the DP of an SU-8 -coated p-type FET, respectively. The I_{DD} through n-doped FET is lowest at the DP of the n-doped FET, while the I_{DD} through the p-doped FET is lowest at the DP of the

p-doped FET. The DPs of two FETs, the maximum and minimum values of the V_{OUT} transfer curve, match well with the two minimum values of the I_{DD}. Additionally, the lowest measured value of voltage gain ($A = dV_{OUT}/dV_{IN}$) meets at the DPs of two FETs. The highest measured value of voltage gain is $|A| = 0.17$ measured at $V_{DD} = 3.3$ V. The voltage gain increases with supply voltage. The highest value locates approximately halfway between the DPs of the two FETs.

CONCLUSIONS

We have demonstrated that spontaneous ordering of dipolar polymer segments mediated by π-interactions may establish highly stable complementary doping of graphene. Area-selective polymer doping in conjunction with conventional photolithography accomplished an ambient-stable graphene inverter that shares an electrode between p-type and n-type FETs. This scheme is consistent with the CMOS inverters and offers a large degree of freedom in designing graphene-based electronics, including logic circuits. It is noteworthy that we employed a back gate regime through a thick (300 nm) SiO_2 gate insulator. Subsequent employment of a top-gate regime with thinner insular[19] or double-gate regime[20] could attain a gain value of more than 1, which is generally considered as a standard performance for practical devices. Furthermore, along with our current research effort for semiconducting graphene preparation,[50] this straightforward polymer doping can be exploited for various graphene-based electronics with improved switching and rectifying performances, particularly in mechanically flexible form.

EXPERIMENTAL METHODS

Polymer Doping Procedure. All reagents and polymers were purchased from Aldrich and used as received. All polymer solutions were prepared at 1 wt % concentration. P4VP (M_n: 60 000 g/mol) was dissolved in methanol, PEG (M_n: 10 000 g/mol) in dichloromethane, PS (M_n: 280 000 g/mol) and PMMA (M_n: 350 000 g/mol) in toluene, and PAN (M_n: 150 000 g/mol) in *N*,*N*-dimethylformamide. PDMS (Sylgard 184 from Dow Corning) was diluted in heptane before using. SU-8 2000.5 was purchased from Microchem and used as received. All polymer solutions were spun on GFETs at 1000 rpm for 60 s, respectively. Thermal annealing of the polymer-doped GFETs was carried out on a temperature-controllable hot plate under ambient conditions.

Polymer-Doped Graphene TFT Fabrication. A chemical vapor deposition (CVD)-grown graphene monolayer was transferred onto standard 300 nm SiO_2/Si wafers. The Si substrate is used as the gate electrode, and the oxide serves as the gate dielectric. The graphene film was patterned by O_2 RIE etching with a shadow mask. Au source and drain electrodes with a 60 μm gap distance are deposited on the patterned graphene. Polymer doping layers were spin-casted onto the graphene channel and thermally annealed at 100−150 °C.

Polymer-Doped Graphene Inverter Fabrication. See Supplementary Figure S9.

Material and Device Characterization. A UV−vis spectrometer (V530, Jasco) was utilized to measure the absorbance of P4VP films with and without graphene on quartz plates. Raman spectroscopy of graphene was measured by using a high-resolution dispersive Raman microscope (ARAMIS, Horiba Jobin Yvon). For electrical property characterization, the 20 nm Au source and drain electrodes were deposited on 100 μm stripe-patterned graphene using an e-beam evaporator (pressure $\cong 10^{-6}$ Torr) with a shadow mask. The electrical performances of devices were measured under air ambient condition using precision semiconductor parameter analyzers (HP 4156A for GFET and HP 4155B for inverters).

Conflict of Interest: The authors declare no competing financial interest.

Acknowledgment. This work is principally supported by the Institute for Basic Science (IBS) [CA1301-02]. E.-S.L. and Y.-H.K. were supported by the Global Frontier R&D (2011-0031566) program through the NRF of Korea.

Supporting Information Available: Experimental section, dipole moments of each repeating unit of graphene-doped materials, Raman spectrum of monolayer graphene, *I*−*V* curves of graphene FETs to be doped with various polymers, DOS theories of polymer-doped graphene, and graphs of electrical switching characteristics of graphene inverters. This material is available free of charge *via* the Internet at http://pubs.acs.org.

REFERENCES AND NOTES

1. Lin, Y. M.; Dimitrakopoulos, C.; Jenkins, K. A.; Farmer, D. B.; Chiu, H.-Y.; Grill, A.; Avouris, P. 100-GHz Transistors from Wafer-Scale Epitaxial Graphene. *Science* **2010**, *327*, 662.
2. Lee, S. H.; Lee, D. H.; Lee, W. J.; Kim, S. O. Tailored Assembly of Carbon Nanotubes and Graphene. *Adv. Funct. Mater.* **2011**, *21*, 1338–1354.
3. Novoselov, K. S.; Geim, A. K.; Morozov, S. V.; Jiang, D.; Katsnelson, M. I.; Grigorieva, I. V.; Dubonos, S. V.; Firsov, A. A. Two-Dimensional Gas of Massless Dirac Fermions in Graphene. *Nature* **2005**, *438*, 197–200.
4. Xia, F.; Farmer, D. B.; Lin, Y.; Avouris, P. Graphene Field-Effect Transistors with High On/Off Current Ratio and Large Transport Band Gap at Room Temperature. *Nano Lett.* **2010**, *10*, 715–718.
5. Novoselov, K. S.; Jiang, D.; Zhang, Y.; Morozov, S. V.; Stormer, H. L.; Zeitler, U.; Maan, J. C.; Boebinger, G. S.; Kim, P.; Geim, A. K. Room-Temperature Quantum Hall Effect in Graphene. *Science* **2007**, *315*, 1379.
6. Schall, D.; Otto, M.; Neumaier, D.; Kurz, H. Integrated Ring Oscillators Based on High-Performance Graphene Inverters. *Sci. Rep.* **2013**, *3*, 2592.
7. Echtermeyer, T. J.; Lemme, M. C.; Baus, M.; Szafranek, B. N.; Geim, A. K.; Kurz, H. Nonvolatile Switching in Graphene Field-Effect Devices. *IEEE Electron Device Lett.* **2008**, *29*, 952–954.
8. Maiti, U. N.; Lee, W. J.; Lee, J. M.; Oh, Y. T.; Kim, J. Y.; Kim, J. E.; Shim, J. W.; Han, T. H.; Kim, S. O. 25th Anniversary Article: Chemically Modified/Doped Carbon Nanotubes & Graphene for Optimized Nanostructures and Nanodevices. *Adv. Mater.* DOI: 10.1002/adma.201303265.
9. Ci, L.; Song, L.; Jin, C.; Jariwala, D.; Wu, D.; Li, Y.; Srivastava, A.; Wang, Z. F.; Storr, K.; Balicas, L.; *et al*. Atomic Layers of Hybridized Boron Nitride and Graphene Domains. *Nat. Mater.* **2010**, *9*, 430–435.
10. Park, S. J.; Hu, Y.; Hwang, J. O.; Lee, E.; Casabianca, L. B.; Cai, W.; Potts, J. R.; Ha, H.; Chen, S.; Oh, J.; *et al*. Chemical Structures of Hydrazine-Treated Graphene Oxide and Generation of Aromatic Nitrogen Doping. *Nat. Commun.* **2012**, *3*, 638.
11. Hwang, J. O.; Park, J. S.; Choi, D. S.; Kim, J. Y.; Lee, S. H.; Lee, K. E.; Kim, Y.; Song, M. H.; Yoo, S.; Kim, S. O. Workfunction-Tunable, N-Doped, Reduced Grahene Transparent Electrodes for High-Performance Polymer Light-Emitting Diodes. *ACS Nano* **2012**, *6*, 159–167.
12. Castro Neto, A. H.; Guinea, F.; Peres, N. M. R.; Novoselov, K. S.; Geim, A. K. The Electronic Properties of Graphene. *Rev. Mod. Phys.* **2009**, *81*, 109–162.
13. Crowther, A. C.; Ghassaei, A.; Jung, N.; Brus, L. E. Strong Charge-Transfer Doping of 1 to 10 Layer Graphene by NO_2. *ACS Nano* **2012**, *6*, 1865–1875.

14. Chen, W.; Chen, S.; Qi, D. C.; Gao, X. Y.; Wee, A. T. S. Surface Transfer p-Type Doping of Epitaxial Graphene. *J. Am. Chem. Soc.* **2007**, *129*, 10418–10422.
15. Movva, H. C. P.; Ramon, M. E.; Corbet, C. M.; Sonde, S.; Chowdhury, S. F.; Carpenter, G.; Tutuc, E.; Banerjee, S. K. Self-Aligned Graphene Feld-Effect Transistors with Polyethyleneimine Doped Source/Drain Access Regions. *Appl. Phys. Lett.* **2012**, *101*, 183113.
16. Schenin, F.; Geim, A. K.; Morozov, S. V.; Hill, E. W.; Blake, P.; Katsnelson, M. I.; Novoselov, K. S. Detection of Individual Gas Molecules Adsorbed on Graphene. *Nat. Mater.* **2007**, *6*, 652–655.
17. Ho, P.; Yeh, Y.; Wang, D.; Li, S.; Chen, H.; Chung, Y.; Lin, C.; Wang, W.; Chen, C. Self-Encapsulated Doping of n-Type Graphene Transistors with Extended Air Stability. *ACS Nano* **2012**, *6*, 6215–6221.
18. Traversi, F.; Russo, V.; Sordan, R. Integrated Complementary Graphene Inverter. *Appl. Phys. Lett.* **2009**, *94*, 223312.
19. Rizzi, L. G.; Bianchi, M.; Behnam, A.; Carrion, E.; Guerriero, E.; Polloni, L.; Pop, E.; Sordan, R. Cascading Wafer-Scale Integrated Graphene Complementary Inverters under Ambient Conditions. *Nano Lett.* **2012**, *12*, 3948–3953.
20. Chen, H.; Appenzeller, J. Complementary-Type Graphene Inverters Operating at Room-Temperature. *IEEE DRC 2011 69th Annual* **2011**, 33–34.
21. Kuo, S. W.; Wu, C. H.; Chang, F. C. Thermal Properties, Interactions, Morphologies, and Conductivity Behavior in Blends of Poly(vinylpyridine)s and Zinc Perchlorate. *Macromolecules* **2004**, *37*, 192–200.
22. Chen, J.; Jang, C.; Xiao, S.; Ishigami, M.; Fuhrer, M. S. Intrinsic and Extrinsic Performance Limits of Graphene Devices on SiO_2. *Nat. Nanotechnol.* **2008**, *3*, 206–209.
23. Ryu, S.; Liu, L.; Berciaud, S.; Yu, Y.; Liu, H.; Kim, P.; Flynn, G. W.; Brus, L. E. Atmospheric Oxygen Binding and Hole Doping in Deformed Graphene on a SiO_2 Substrate. *Nano Lett.* **2010**, *10*, 4944–4951.
24. Katsnelson, M. I. Graphene: Carbon in Two Dimensions. *Mater. Today* **2006**, *10*, 20–27.
25. Allen, M. J.; Tung, V. C.; Kaner, R. B. Honeycomb Carbon: A Review of Graphene. *Chem. Rev.* **2010**, *110*, 132–145.
26. Geim, A. K.; Novoselov, K. S. The Rise of Graphene. *Nat. Mater.* **2007**, *6*, 183–191.
27. Zhang, Y.; Tan, W.; Stormer, H. L.; Kim, P. Experimental Observation of the Quantum Hall Effect and Berry's Phase in Graphene. *Nature* **2005**, *438*, 201–204.
28. Chen, S.; Cai, W.; Chen, D.; Ren, Y.; Li, X.; Zhu, Y.; Ruoff, R. S. Adsorption/Desorption and Electrically Controlled Flipping of Ammonia Molecules on Graphene. *New J. Phys.* **2010**, *12*, 125011.
29. Suk, J. W.; Lee, W. H.; Lee, J.; Chou, H.; Piner, R. D.; Hao, Y.; Akinwande, D.; Ruoff, R. S. Enhancement of the Electrical Properties of Graphene Grown by Chemical Vapor Deposition *via* Controlling the Effects of Polymer Residue. *Nano Lett.* **2013**, *13*, 1462–1467.
30. Ferrari, A. C.; Basko, D. M. Raman Spectroscopy as a Versatile Tool for Studying the Properties of Graphene. *Nat. Nanotechnol.* **2013**, *8*, 235–246.
31. Ferrari, A. C.; Meyer, J. C.; Scardaci, V.; Casiraghi, C.; Lazzeri, M.; Mauri, F.; Piscanec, S.; Jiang, D.; Novoselov, K. S.; Roth, S.; *et al*. Raman Spectrum of Graphene and Graphene Layers. *Phys. Rev. Lett.* **2006**, *97*, 187401.
32. Sojoudi, H. Impact of Post-Growth Thermal Annealing and Environmental Exposure on the Unintentional Doping of CVD Graphene Films. *J. Vac. Sci. Technol. B* **2012**, *30*, 041213.
33. Yan, J.; Zhang, Y.; Kim, P.; Pinczuk, A. Electric Field Effect Tuning of Electron-Phonon Coupling in Graphene. *Phys. Rev. Lett.* **2007**, *98*, 166802.
34. Huang, M.; Yan, H.; Chen, C.; Song, D.; Heinz, T. F.; Hone, J. Phonon Softening and Crystallographic Orientation of Strained Graphene Studied by Raman Spectroscopy. *Proc. Natl. Acad. Sci. U.S.A.* **2009**, *106*, 7304–7308.
35. Wei, P.; Liu, N.; Lee, H. R.; Adijanto, E.; Ci, L.; Naab, B. D.; Zhong, J. Q.; Park, J.; Chen, W.; Cui, Y.; Bao, Z. Tuning the Dirac Point in CVD-Grown Graphene through Solution Processed n-Type Doping with 2-(2-Methoxyphenyl)-1,3-dimethyl-2,3-dihydro-1*H*-benzoimidazole. *Nano Lett.* **2013**, *13*, 1890–1897.
36. Kaljurand, I.; Rodima, T.; Leito, I.; Koppel, I. A.; Schwesinger, R. Self-Consistent Spectrophotometric Basicity Scale in Acetonitrile Covering the Range between Pyridine and DBU. *J. Org. Chem.* **2000**, *65*, 6202–6208.
37. Blöchl, P. E. Projector Augmented-Wave Method. *Phys. Rev. B* **1994**, *50*, 17953–17979.
38. Perdew, J. P.; Burke, K.; Ernzerhof, M. Generalized Gradient Approximation Made Simple. *Phys. Rev. Lett.* **1996**, *77*, 3865–3868.
39. Kresse, G.; Joubert, D. From Ultrasoft Pseudopotentials to the Projector Augmented-Wave Method. *Phys. Rev. B* **1999**, *59*, 1758–1775.
40. Kim, Y. -H.; Heben, M. J.; Zhang, S. B. Nanotube Wires on Commensurate InAs Surface: Binding Energies, Band Alignments, and Bipolar Doping by the Surfaces. *Phys. Rev. Lett.* **2004**, *92*, 176102.
41. Kim, Y. -H.; Zhang, S. B.; Yu, Y.; Xu, L. F.; Gu, C. Z. Dihydrogen Bonding, p-Type Conductivity, and Origin of Change in Work Function of Hydrogenated Diamond (001) Surfaces. *Phys. Rev. B* **2006**, *74*, 075329.
42. Fratini, S.; Guinea, F. Substrate-Limited Electron Dynamics in Graphene. *Phy. Rev. B* **2008**, *77*, 195415.
43. Hwang, E. H.; Adam, S.; Sarma, S. D. Carrier Transport in Two-Dimensional Graphene Layers. *Phys. Rev. Lett.* **2007**, *98*, 186806.
44. Chen, F.; Xia, J.; Tao, N. Ionic Screening of Charged-Impurity Scattering in Graphene. *Nano Lett.* **2009**, *9*, 1621–1625.
45. Chen, F.; Xia, J.; Ferry, D. K.; Tao, N. Dielectric Screening Enhanced Performance in Graphene FET. *Nano Lett.* **2009**, *9*, 2571–2574.
46. Jang, C. Tuning the Effective Fine Structure Constant in Graphene: Opposing Effects of Dielectric Screening on Short- and Long-Range Potential Scattering. *Phys. Rev. Lett.* **2008**, *101*, 146805.
47. Chen, J.-H.; Jang, C.; Adam, S.; Fuhrer, M. S.; Williams, E. D.; Ishigami, M. Charged-Impurity Scattering in Graphene. *Nat. Phys.* **2008**, *4*, 377–381.
48. Kim, S. M.; Jang, J. H.; Kim, K. K.; Park, H. K.; Bae, J. J.; Yu, W. J.; Lee, I. H.; Kim, G.; Loc, D. D.; Kim, U. J.; *et al*. Reduction-Controlled Viologen in Bisolvent as an Environmentally Stable *n*-Type Dopant for Carbon Nanotubes. *J. Am. Chem. Soc.* **2009**, *131*, 327–331.
49. Farmer, D. B.; Lin, Y.-M.; Afzali-Ardakani, A.; Avouris, P. Behavior of a Chemically Doped Graphene Junction. *Appl. Phys. Lett.* **2009**, *94*, 213106.
50. Kim, J. Y.; Kim, B. H.; Hwang, J. O.; Jeong, S.-J.; Shin, D. O.; Mun, J. H.; Choi, Y. J.; Jin, H. M.; Kim, S. O. Flexible and Transferrable Self-Assembled Nanopatterning on Chemically Modified Graphene. *Adv. Mater.* **2013**, *25*, 1331–1335.